This is a repository copy of *Molecular Structure Control in Mesophase Pitch via Co-Carbonization of Coal Tar Pitch and Petroleum Pitch for Production of Carbon Fibers with Both High Mechanical Properties and Thermal Conductivity*.

White Rose Research Online URL for this paper:
https://eprints.whiterose.ac.uk/160330/

Version: Accepted Version

Molecular Structure Control in Mesophase Pitch via Co-carbonization of Coal Tar Pitch and Petroleum Pitch for Production of Carbon Fibers with both High Mechanical Properties and Thermal Conductivity

Jianguang Guo,[†,‡] Xuanke Li,[*,†,‡,§] Huitao Xu,[†,‡] Hui Zhu,[§] Baoliu Li,[†,‡] and Aidan Westwood[*,⊥]

[†]College of Materials Science and Engineering, Hunan University, Changsha, 410082, People's Republic of China

[‡]Hunan Province Key Laboratory for Advanced Carbon Materials and Applied Technology, Hunan University, Changsha, 410082, People's Republic of China

[§]State Key Laboratory of Refractories and Metallurgy, Wuhan University of Science and Technology, Wuhan, Hubei, 430081, People's Republic of China

[⊥]School of Chemical and Process Engineering, University of Leeds, Leeds, LS2 9JT, United Kingdom

[*]E-mail: xkli8524@sina.com (X.K. Li).   A.V.K.Westwood@leeds.ac.uk (A. Westwood)

Abstract: Spinnable mesophase pitches C-MP, P-MP and C/P-MP were synthesized from coal tar pitch, petroleum pitch and their co-carbonized pitches, respectively. The molecular structures of these mesophase pitches and their effect on the microcrystalline sizes of the mesophase and the properties of carbon fibers derived from them were comparatively investigated. The molecular structures and orientation of the prepared mesophase pitches have significant influence on the performance of resultant carbon fibers. In comparison with P-MP and C/P-MP, C-MP possessing the highest aromaticity, a rigid molecular structure and a very small amount of methyl groups makes C-MP-CFs with smaller crystal size and lower decomposition during the preparation process, thus results in best mechanical properties of their carbon fibers, consequently. The prepared P-MP, however, containing abundant methyl groups

1

and possessing a semi-rigid molecular structure, yields products with higher d_{002}-spacing and larger mesomorphic phase size. The largest crystallite dimension of P-MP combined with its higher molecular orientation makes P-MP-CFs possessing the highest crystal size and axial thermal conductivity. On the other hand, C/P-MP shows the molecular structure character of both coal tar pitch and petroleum pitch and a tunable mesophase domain orientation. The carbon fiber prepared from co-carbonized C/P-MP shows both good mechanical properties, like C-MP-based fiber, and, in particular, ultrahigh thermal conductivity, like P-MP-based fiber.

1. Introduction

Highly oriented carbon fibers with high thermal conductivity are usually prepared from mesophase pitches [1-2]. The high thermal conductivity and ultrahigh tensile modulus of mesophase pitch-based carbon fibers are attributable to the highly oriented aromatic molecules with planar liquid crystal structure in the parent mesophase pitches [3]. The design and modification of the precursors' chemical composition and molecular structure play an important role in control of the planar molecules' sizes and the rheological properties (related to alkyl group content of these aromatic molecules) in mesophase pitches [4-8].

In order to study control the molecular weight distribution and aromatic molecules' planar structure in mesophase pitches, selected model aromatic hydrocarbons, such as naphthalene, anthracene and methylnaphthalene, have been used in preparation of mesophase pitches by a catalytic synthesis process [9-13]. Carbon fibers, possessing excellent performance, were then prepared from these synthesized mesophase pitches. This work suggests that the presence of methyl groups effectively improves the

orientation of aromatic molecules in mesophase pitch and facilitates the preparation of carbon fiber with high tensile modulus and large grain size [12].

Mesophase pitch-based carbon fibers with high performance have been commercialized successfully. However, little information about the preparation process and properties of spinnable mesophase pitches from coal tar pitch (CP) or petroleum pitch (PP) was reported [14]. Since coal tar pitch and petroleum pitch are composed of thousands of compounds [15,16], with wide molecular weight distribution and poorly defined chemical structure [14], the fabrication process design and the synthesis control of spinnable mesophase pitches from these two kinds of pitches are not easy [17]. Researchers usually explain the properties of mesophase pitches through the characterization of their main chemical structure and optical texture features, such as average molecular weight, aromaticity, hydrogen and carbon distribution as well optical texture. The rheological and spinning properties of the mesophase pitches are largely due to the naphthenic structures and alkyl groups of their feedstocks [10,18]. The research papers on comparison/blending of coal-tar and petroleum pitch are mainly focused on the mesophase pitch preparation and their application as graphitizable carbons [19-21]. Even though it has practical importance in explaining the effects of precursor chemical structure on carbon fiber properties, few reports look into the molecular irregularity and resulting microcrystalline (im)perfection of mesophase pitches prepared from differing feedstocks. In our previous work, a spinnable mesophase pitch was prepared from two precursors by taking advantages of both of abundant naphthenic structures in synthetic naphthalene pitch and of aliphatic groups in FDO [18]. In order to further reveal the effect of molecular structure and stacking on mesophase pitch texture and derived carbon fiber properties, three kinds of spinnable mesophase pitches were prepared from coal tar pitch, petroleum pitch and their

3

blends, respectively. The molecular structure (aromaticity and aliphatic groups), anisotropic domain and crystallite dimensions of the mesophase pitches and the properties of resultant carbon fibers were investigated in this work. Mesophase pitch was synthesized by co-carbonization of coal tar pitch and petroleum pitch to accomplish its molecular structure control and carbon fibers combining the advantages of coal tar mesophase pitch-based carbon fibers and petroleum mesophase pitch-based carbon fibers were prepared from this designed mesophase pitch.

2. Experimental

2.1. Preparation of spinnable mesophase pitches

A commercial impregnated CP provided by Jining carbon group co., Ltd and a PP provided by China Petrochemical Group Co., Ltd prepared from high temperature distillation of FCC slurry were used as the feedstocks to prepare spinnable mesophase pitches. The properties of CP and PP are shown in Table 1. The two feedstocks contain less than 1 wt.% of quinoline insoluble (QI) content.

Table 1 General properties and chemical composition of CP and PP.

| Sample | SP[a]/°C | TS[b]/% | Elemental content/wt.% | | | | H/C |
			C	H	N	S	
CP	87	62.55	93.20	4.49	1.08	0.53	0.578
PP	108	81.31	93.40	5.57	0.25	0.76	0.716

[a] Softening point tested by ring and ball method, [b] Toluene soluble

The preparation of mesophase pitches consisted of the feedstocks' pressurized heat treatment followed by thermal polymerization under nitrogen flow with stirring [20,22]. The CP, PP and their

blends in 50:50 wt.% proportions were used as the basic feedstocks. The optimized pressurized heat treatment was conducted using a 300 mL autoclave at 430 °C for 6 h under 3~5 MPa reaction pressure. The heat-treated pitch was transferred to a stainless steel reactor with an agitator. The pitch was then vigorously stirred during heat treatment at 410 °C and nitrogen was bubbled through from the bottom at a specific flow rate of 6 mL/min/g (mass of pitch). After the treatment, mesophase pitch was produced and cooled down naturally under flowing nitrogen. The mesophase pitches prepared from CP, PP and their blends were named C-MP, P-MP and C/P-MP, respectively.

2.2. Preparation of mesophase pitch-based carbon fiber

Mesophase pitch-based fiber was prepared from each pitch at temperatures about 80 °C higher than the pitch softening points by melt spinning from a circular shaped spinneret (D = 0.2mm, L/D=3) under 0.2 MPa nitrogen pressure with a drawing speed of 400 m/min. In order to decrease the oxidative stabilization time, the as-spun mesophase pitch fibers underwent a heating rate of 5 °C/min to 160 °C and then a heating rate of 0.5 °C /min to 280 °C for 1h under flowing air atmosphere as the optimized stabilized condition. Subsequently, the stabilized fibers were carbonized at 1000 °C for 30 min at a heating rate of 5 °C/min and then the carbon fibers were further graphitized at 3000 °C for about 10 min.

2.3. Characterization of mesophase pitch and carbon fiber therefrom

The SP of mesophase pitches was tested using a capillary rheometer (CFT-100EX, Shimadzu). The fractional composition of the mesophase pitches was analysed by sequential Soxhlet extraction with toluene (T), tetrahydrofuran (THF) and quinoline (Q) solvents. The optical texture of the mesophase pitches were observed using a polarized microscope (POM, BX53M, Olympus) and the anisotropic

5

content was determined by the measuring module of the microscope's own software. To prepare samples for this each mesophase pitch was annealed at temperatures about 80 °C higher than its softening point for 1 h under a nitrogen gas flow and cooled naturally [21], and then polished for texture observation under polarized light.

The elemental contents (C, H, N and S) of the samples was analysed using an elemental analyzer (Vario EL III, Elementar) and the oxygen content was determined by difference (O=100-C-H-N-S). The functional groups in the feedstocks and mesophase pitches were characterized by FT-IR (IS10, Thermo Fisher). The chemical structure of the mesophase pitches was identified by solid-state ^{13}C-NMR (600 DD2, Aglient). This NMR analysis was performed at a resonance frequency of 150.15 MHz and recorded with spinning rate of 15 KHz with a 4 mm probe at room temperature. A delay time of 5s was used over 2048 scans. Carbon in ^{13}C-NMR was classified according to the chemical shifts into seven categories: CH_3, methyl carbons, 17–23 ppm; CH_2, methylene carbons in alkyl chains, 23–34 ppm; CH_{a2}, methylene carbons in the position to two aromatic rings, 34–50 ppm; CH_{ar}, protonated aromatic carbons, 108–115 ppm; Car3, peri-condensed aromatic carbons, 115–129.5 ppm; C_{ar}^s, aromatic carbons with aliphatic chains substituents, 129.5–132.5 ppm; C_{ar2}, cata-condensed aromatic carbons or aromatic carbons with aromatic substituents, 132.5–160 ppm [23,24].

The oxidization behavior of the as-spun mesophase pitch fibers was followed from room temperature to 400 °C with a heating rate of 2 °C/min under air atmosphere using a thermogravimetric analysis (TGA) system (STA 409 PC, Netzsch).

The Raman spectra of the samples were collected using a Raman spectrometer (HR Evolution, HORIBA) with a Nd laser (λ=532 nm) at 3.2 mW.

In order to accurately determine the changes in d_{002}-spacing and carbon layer stacking height (L_c) for carbon fibers prepared from different mesophase pitches and heat-treatment temperatures, the XRD patterns were collected in a scanning range (2θ) of 22 to 30° with a scanning rate of 1°/min using Cu K_α radiation. The d_{002}-spacing and L_c values of mesophase pitches were calculated with reference to the standard method reported by the Japanese Society for the Promotion of Science [25]. Based on the Bragg equation [26] and the Scherrer's equation [27], the d_{002}-spacing and L_c values of carbon fibers were calculated, respectively. Since the (110) plane diffraction peak of graphite fibers are very weak owing to their highly oriented crystal structure, their La values were calculated by the equation (1) [28]

$$L_a=0.95/(d_{002}-0.3354) \qquad (1)$$

The morphology and microstructure of the carbon fibers were observed using a JSM-6700F scanning electron microscope (SEM)) and a Tecnai G2 F20 S-TWIN high resolution transmission electron microscope (HRTEM). The electrical resistivities (ρ), tensile Strength (TS) and tensile modulus (TM) of the graphitized carbon fibers were measured with reference to the previous paper [29]. The broken carbon fibers were numbered and the corresponding diameter of each carbon fiber was further measured under SEM in order to calculate the mechanical properties of the carbon fiber.

3. Results and discussion

3.1. Molecules structure analysis of the feedstocks by FT-IR

Fig. 1 shows the FT-IR spectra of the two feedstocks. Both the CP and PP exhibited moderate aromatic C-H stretching bands at 3030 cm^{-1}. In comparison with PP showing strong aliphatic C-H stretching peaks at around 2920 and 2860 cm^{-1}, CP shown much less intense aliphatic C-H stretching bands, which is highly consistent with the result reported in Ref. [30]. In addition, the FT-IR spectra shown in Fig.1

show that, compared to CP, PP shows an obviously stronger signal for methyl groups absorbing at 1380

cm^{-1}. The CP, being mainly composed of unsubstituted large polyaromatic hydrocarbons (PAH), shows

a much higher ratio of aromatic to aliphatic C-H stretching bands than PP, which has a higher content

of alkyl-substituted aromatic species [31]. The higher I_{750}/I_{880} ratio of four-adjacent hydrogens (quatro)

at 750 cm^{-1} to isolated hydrogens (solo) at 880 cm^{-1} for CP, compared with PP, which can be calculated

from Fig. 1, also suggests that CP possesses higher aromaticity and PP has more aliphatic groups.
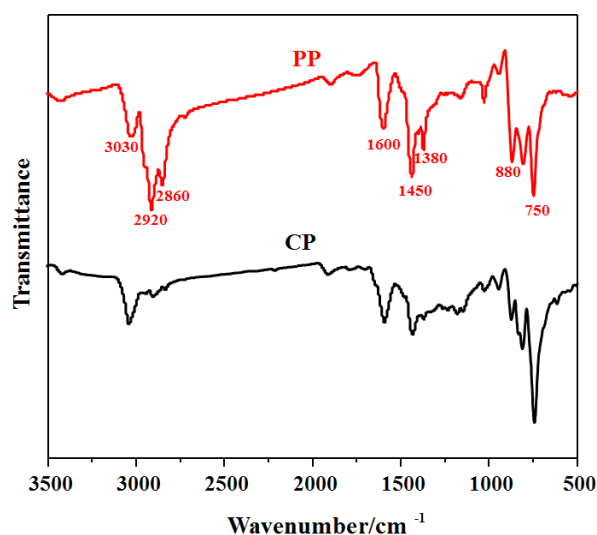

Fig. 1 FT-IR spectra of the two feedstocks.

3.2. Property and optical morphology analysis of the mesophase pitches

Some general properties of the three products after thermal polymerization were summarized in Table

2. P-MP tends to have the lowest softening point, the highest TS and THFS values and the lowest QI

value. C-MP exhibits the highest softening point and fixed carbon (FC) content as well as the lowest

H/C atomic ratio, which has a close relation with its higher aromaticity. However, C/P-MP has an

intermediate softening point, QI, THFS and TS value, as well as an intermediate FC content and H/C

ratio to compared to those of the other pitches. The values for C/P-MP could be attributed to the high

8

aromaticity of CP and the abundant aliphatic groups of PP as well as to interactions between the two feedstocks during the co-carbonization.

Table 2 Some general properties of the mesophase pitches.

Sample	SP/°C	FC[c]/%	TS/%	THFS[d]/%	QI[e]/%	n(H)/n(C)
C-MP	276	92.80	9.67	17.44	68.22	0.478
C/P -MP	270	90.03	20.82	34.11	51.81	0.503
P-MP	262	87.25	23.32	36.70	46.72	0.530

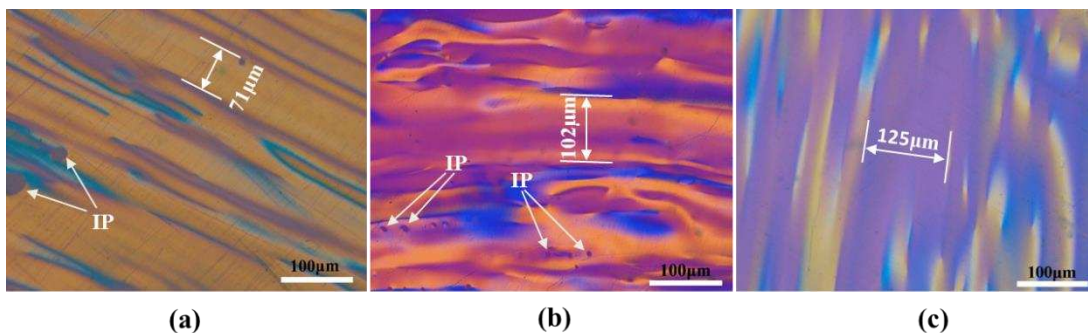[c] Fixed carbon content, [d] Tetrahydrofuran soluble, [e] Quinoline insoluble

Fig. 2 Optical micrographs of (a) C-MP, (b) C/P-MP and (c) P-MP.

Fig. 2 shows the anisotropic contents and optical texture of three mesophase pitches. The anisotropic content of C-MP shown in Fig. 2(a) is more than 95 vol% and an elongated anisotropic flow domain texture was observed, which is different from the mosaic textures of coal tar pitch-based mesophase pitches reported in Ref. [21]. The flow domain texture suggests that C-MP might have good flowability and spinnability [18,21]. The C/P-MP and P-MP display larger size flow domain texture and have an anisotropic content over 98 vol%. The widths of about 71μm, 102μm and 125μm shown in Fig. 2 are typical of the anisotropic domain sizes of C-MP, C/P-MP and P-MP, respectively. The larger anisotropic

texture size and content of C/P-MP than those of C-MP are attributed to the introduction of short alkyl group (especially methyl groups) and naphthenic structures from PP by co-carbonization process. The transfer of methyl groups and hydrogen from PP promotes the molecule rearrangement of C/P-MP so that the orientation of C/P-MP becomes more orderly than that of C-MP [6, 21], thus enhances the solubility and fusibility of C/P-MP.

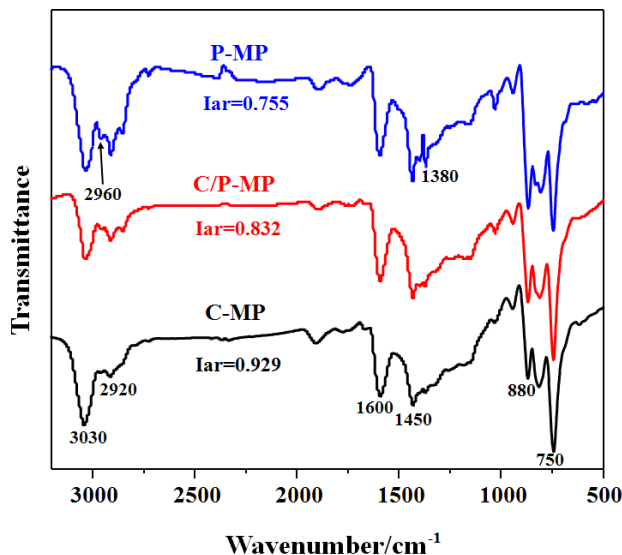3.3. Molecules structure analysis of mesophase pitch

Fig. 3 FT-IR spectra of the prepared mesophase pitches.

Fig. 3 shows the FT-IR spectra of the three mesophase pitches. Some obvious differences can be observed in the absorption peaks at 2900-3000 cm^{-1}, 1450 cm^{-1} and 1380 cm^{-1}, ascribed to the different aliphatic groups content in the mesophase pitches. All the peaks of P-MP, especially around 2960 cm^{-1} (asymmetric CH_3 stretching [31]) and 1380 cm^{-1}, are more intense than those of C/P-MP and C-MP, suggesting more methyl groups (-CH_3) in P-MP than in the other two mesophase pitches. The aromaticity index (I_{ar}) was calculated using the formula: $I_{ar} = Abs_{3030} / (Abs_{3030} + Abs_{2920})$ [25] where Abs_{3030} and Abs_{2920} represent the absorption peak areas at around 3030 and 2920 cm^{-1}, respectively,

10

obtained by deconvolution [31]. The I_{ar} index for C-MP, C/P-MP and P-MP was 0.929, 0.832 and 0.755, respectively. This indicates that C/P-MP prepared by co-carbonization possesses more aliphatic groups than C-MP.
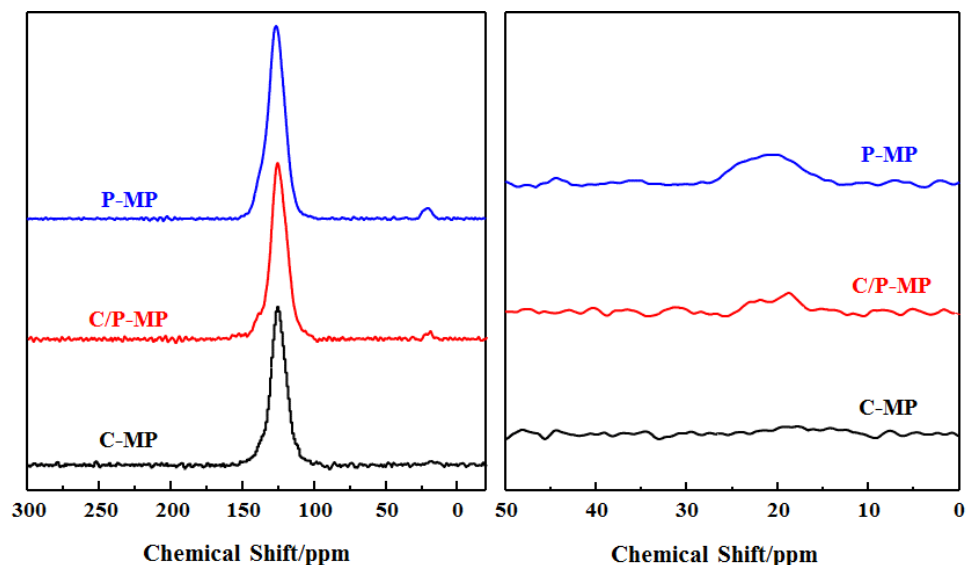

Fig. 4 Solid-state ^{13}C-NMR spectra of the mesophase pitches.

Table 3 Carbon distributions of the resultant mesophase pitches from analysis of solid-state ^{13}C-NMR spectra.

Sample	Aliphatic/%			Aromatic/%				C_{ar3}/C_{ar2}	Fa
	CH_3 [f]	CH_2 [g]	Ch_{a2} [h]	CH_{ar} [i]	C_{ar3} [j]	$C_{ar}s$ [k]	C_{ar2} [l]		
C-MP	2.24	1.88	0.88	5.05	66.69	9.46	13.80	4.83	0.95
C/P-MP	7.33	2.45	1.22	4.57	62.80	8.49	13.16	4.77	0.89
P-MP	11.03	3.14	1.83	2.59	50.80	12.97	17.60	2.88	0.84

Fig. 4 shows ^{13}C-NMR spectra of the three mesophase pitches. The molecular architecture of the mesophase pitches was further quantitatively identified and summarized in Table 3. As expected, the

effect of chemical structure such as the shape and rigidity of mesophase pitch molecules, on their molecular orientation and rheological properties [14] might have further influence the properties of the pitches' carbon fiber derivatives [32]. The three mesophase pitches show an aromaticity index (Fa) trend of C-MP > C/P-MP > P-MP, while the aliphatic content is in the reverse order, as shown in Table 3. This suggests that C-MP is mainly composed of rigid aromatic mesogenic units while the P-MP possessed a semi-rigid structure and its various mesogenic units are connected by aryl-aryl bonds or alkyl groups [14]. The C_{ar3}/C_{ar2} parameter gives a measure of the relationship between peri- and cata-condensation [23]. A higher value of C_{ar3}/C_{ar2} indicates more peri-condensation in the molecule structure.

Among the three mesophase pitches, the similar C_{ar3}/C_{ar2} values suggests that C/P-MP possesses a rigid aromatic mesogenic units like C-MP. The lowest C_{ar3}/C_{ar2} value, for P-MP, implies its tendency towards a more linear molecular structure. The aliphatic groups in the mesophase pitches are mainly methyl groups, as shown in Table 3. In particular, the higher aromaticity value and -CH_3 content of C/P-MP indicates that it largely consists of rigid aromatic mesogenic units which contain a moderate number of short aliphatic chains. These results are highly consistent with the FT-IR analyses of the three mesophase pitches. Based on the above results, the typical molecular structures of the three mesophase pitches are represented by the schematic chemical structure shown in Fig. 5 to intuitively reflect the molecular structure difference of three mesophase pitches [23]. The molecular structure of C/P-MP offers the advantages of both rigid aromatic mesogenic units and abundant short aliphatic chains which are inherited from the CP and the PP, respectively.
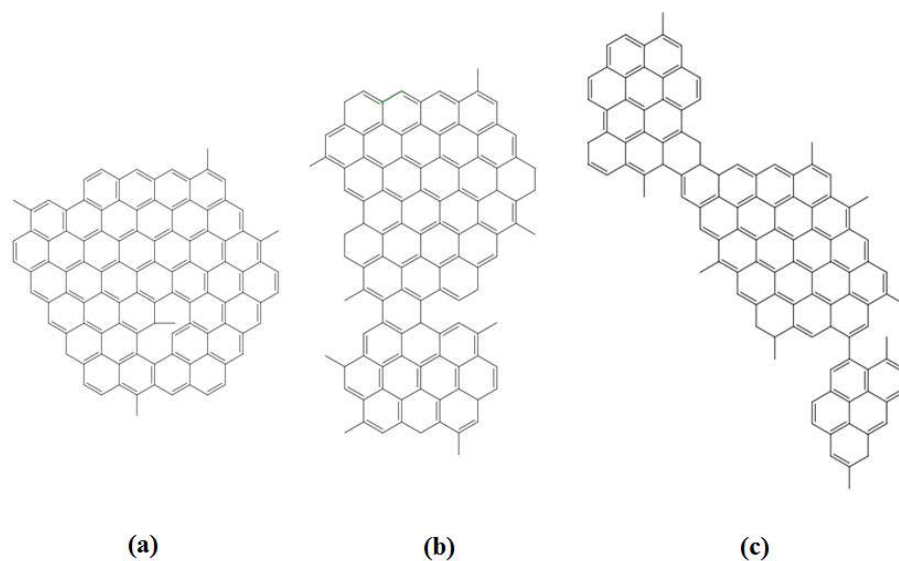
(a)   (b)   (c)

Fig. 5 Schematic molecular representations of the typical chemical structures of C-MP (a), C/P-MP (b) and P-MP (c).

3.4 Molecular orientation and microcrystalline perfection of the mesophase pitches
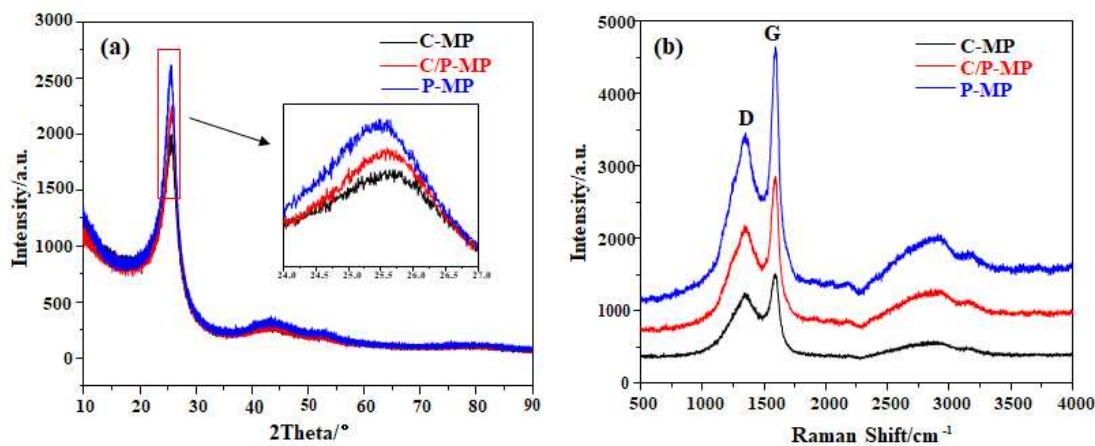

Fig. 6 XRD patterns (a) and Raman spectra (b) of the mesophase pitches.

X-ray diffraction and Raman spectra, used to determine the molecular orientation and microcrystalline perfection of the prepared mesophase pitches, are presented in Fig. 6. Table 4 lists the microcrystalline parameters and the degree of perfection in the molecular arrangement [17] of the mesophase pitches.

13

As presented in Fig. 6 (a), the most obvious diffraction peaks at $2\theta \approx 25.5°$ and $2\theta \approx 43.0°$, corresponding to the d_{002}-spacing and size of aromatic carbon layers, respectively, suggest that the mesophase pitches are highly crystalline [33]. The (002) aromatic carbon layer-planes' peak intensity increases as follows: C-MP < C/P-MP < P-MP, indicating that the stack height (L_c) and the number of aromatic molecular layers (N) increase in the same order, as shown in Table 4. The 2θ angle for the (002) peak, meanwhile, slightly decreases in the order: C-MP > C/P-MP > P-MP (shown in Figure 6(a)), showing d_{002}-spacing increases in order, from C-MP to C/P-MP to P-MP. The molecular stacking heights (L_c) of C-MP, C/P-MP and P-MP are 2.89 nm, 3.12 nm and 3.54 nm, respectively, as shown in Table 4. It is worth noting that these trends for d_{002} and L_c in these prepared mesophase pitches are inconsistent with the result reported in Refs. [4,34], which may be explained by differences in the chemical structure and the rigidity of the mesophase pitch molecules. The semi-rigid molecular structure especially the aryl-aryl single bond, as described in Fig.5(c), reduce the conjugation of P-MP molecules and lead to a certain degree of molecular plane distortion, reducing molecular flatness and hence increasing d_{002}-spacing. Even though this type of C-C single bond will lower the 002 stacking properties of the molecules, the higher molecular stacking（L_c）of P-MP than other pitches, as shown in Table 4, is attributed to the abundant -CH$_3$ groups in P-MP. The -CH$_3$ groups help to increase its molecular mobility and thus promote its molecular stacking height (L_c). This is consistent with the previous conclusion that -CH$_3$ groups resulted in larger and more ordered stacking of the aromatic molecules in mesophase pitch [11-12]. On the other hand, the rigid molecular structure and low amount of -CH$_3$ groups in C-MP, result in its more compact structure through lower interlayer spacings and stack height. The higher L_c value of C/P-MP than that of C-MP is due to its higher -CH$_3$ groups introduced during co-carbonization.

The peak intensity of the Raman D-band and G-band for mesophase pitch is indicative of its molecular character [35]. As shown in Fig. 6 (b), the D-band intensity increases as C-MP < C/P-MP < P-MP. The D-band of P-MP is ascribed to the presence of aryl-aryl C-C bonds and alkyl groups (methyl groups) at the periphery of the molecules [35]. A lower value of I_D/I_G indicates fewer defect sites and hence more highly ordered orientation [14]. The I_D/I_G ratio of C-MP, C/P-MP and P-MP is 0.76, 0.70 and 0.68, respectively. As shown in Table 4, the planar aromatic molecules sizes (L_a) calculated from I_D/I_G increase as C-MP < C/P-MP < P-MP. This demonstrates that the crystalline perfection of C/P-MP is superior to that of C-MP, suggesting that carbon fibers derived from C/P-MP may have larger crystallite dimensions and higher thermal conductivity.

Table 4 Microcrystalline dimension parameters of the three mesophase pitches.

Sample	d_{002}/nm	L_c/nm	N^m	I_D/I_G	L_a^n/nm
C-MP	0.3440	2.89	9.40	0.76	5.79
C/P-MP	0.3452	3.12	10.04	0.70	6.29
P-MP	0.3482	3.54	11.17	0.68	6.47

[m] The layer numbers, $N=L_c/d_{002}+1$, [n] $L_a=44/(I_D/I_G)\times10^{-10}$ m [36]

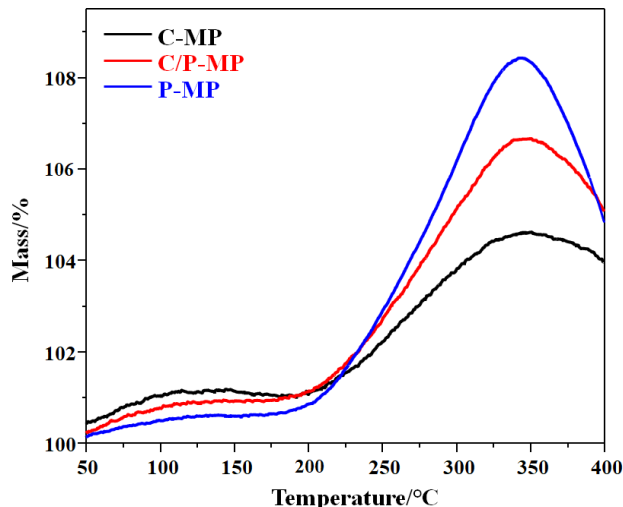3.5 Stabilization optimization and properties of the fibers

Fig. 7 TGA curves of the three as-spun mesophase pitch fibers under air atmosphere.

Fig. 7 shows the TGA curves obtained from the as-spun mesophase pitch fibers to mimic oxidative stabilization at a heating rate of 2 °C/min under air atmosphere. All three curves started to show increase in weight around 180 °C and the as-spun fiber of C-MP, C/P-MP and P-MP reached maximum weight gain respectively of 4.6, 6.7 and 8.4 wt.% at about 340 °C, as indicated in Fig.7. This behavior is determined by the fibres' precursor molecular structure because the stabilization of as-spun mesophase pitch fibers is mainly occurs by the oxidation of hydrogen-containing groups in their molecules [37,38]. The higher H/C atomic ratio and abundant aliphatic groups of P-MP mean that their fully pre-oxidized pitch fibers reached higher oxygen uptake, as shown in Fig. 8. On the other hand, the higher carbonization yield of the pre-oxidized fibers prepared from C/P-MP than that of P-MP indicates that the C/P-MP has a lower decomposition degree during carbonization, suggesting that the mechanical properties of its carbon fibers will be superior than that of P-MP-CFs [39].
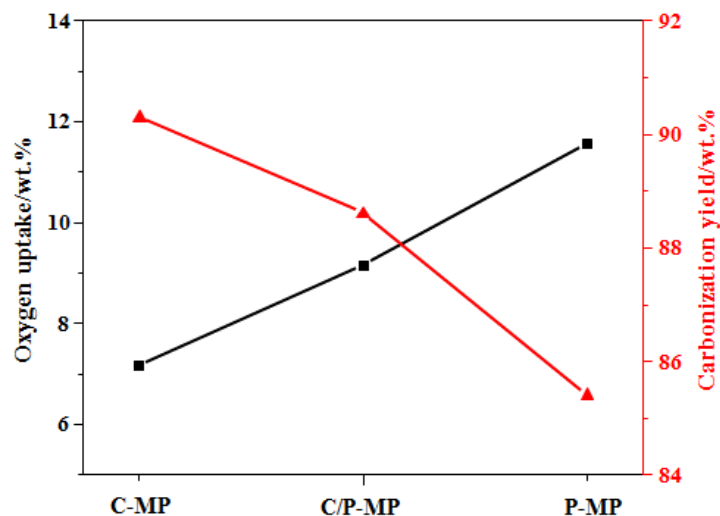
16

Fig. 8 Oxygen uptake content (■) of the three pre-oxidized fibers evaluated by Elemental Analysis and their carbonization yield (▲) at 1000 °C.
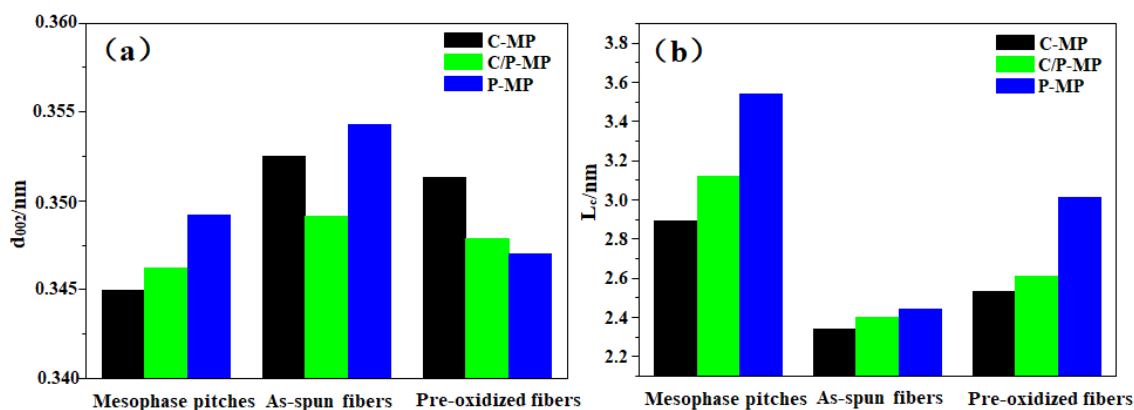

Fig. 9 Changes to the d_{002}-spacing （a）and the L_c value (b), progressing from mesophase pitches to their as-spun fibers and then to pre-oxidized fibers.

XRD was adopted to monitor changes in polyaromatic molecular ordering of the three mesophase pitches during their spinning and stabilization processes. As presented in Fig. 9, the as-spun fibers show higher d_{002}-spacings and lower L_c values than those of their corresponding mesophase pitches, indicating that the crystallites of the mesophase pitches lose some of their stacking during the spinning process [25]. The L_c values of the stabilized fibers are larger than those of the corresponding as-spun fibers, indicating

17

that the reduced stacking is partly recovered during the stabilization process. It's worth noting that the

pre-oxidized fibers prepared from P-MP have even lower d_{002} than that of the mesophase pitch itself as

shown in Fig. 9. This behavior indicates that the pre-oxidation process reduces the distortion of planar

molecules in P-MP and makes these planar molecules more compact by forming a cross-linked structure.
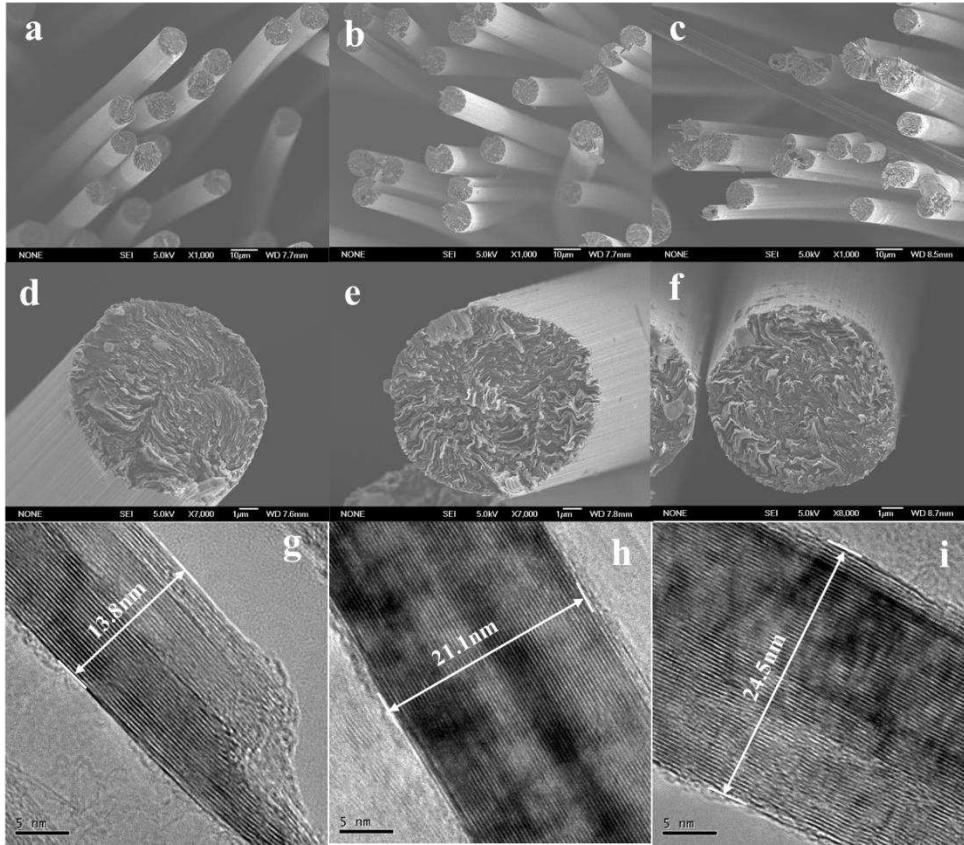

Fig. 10 SEM and HRTEM images of C-MP-CFs (a, d, g), C/P-MP-CFs (b, e, h) and P-MP-CFs (c,

f, i) after graphitization at 3000 °C.

The carbon fibers prepared from mesophase pitches, C-MP, C/P-MP and P-MP were designated C-

MP-CFs, C/P-MP-CFs and P-MP-CFs with diameters of 10.3, 9.8 and 10.0 μm, respectively. As shown

in Fig.10(a), no cracking is observed in the transverse cross-section of C-MP-CFs and these show an

obvious random structure. However, some axial cracks are observed in C/P-MP-CFs and P-MP-CFs as

shown in Fig. 10(b) and Fig. 10(c), respectively, implying better carbon layer orientation in the C/P-MP-CFs and P-MP-CFs. The crystal size of the three carbon fibers increasing in the order: C-MP-CFs < C/P-MP-CFs < P-MP-CFs as shown in their HRTEM images (Fig.10(g), Fig.10(h) and Fig.10(i), respectively), is further confirmed by the XRD (shown in Fig. 11(a)) and patterns and Raman spectra (shown in Fig.11 (b)) analyses. The intensity of the diffraction peaks for the graphite (002) plane of the carbon fibers increases and the I_D/I_G of their Raman spectra decreases going from C-MP-CFs to C/P-MP-CFs to P-MP-CFs, thereby following the same trend as for the precursor pitches. Various properties and crystal lattice parameters of the three carbon fibers are summarized in Table 5. Commercial K13D2U carbon fiber manufactured by Mitsubishi Gas Chemical Co. was used as a reference to compare the performance and crystal parameters of three prepared carbon fibers.
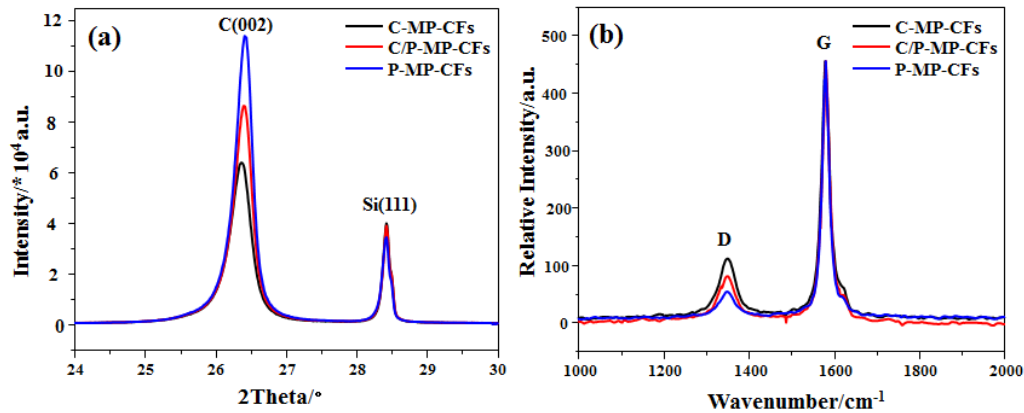

Fig. 11 XRD patterns (a) and Raman spectra (b) of the carbon fibers.

As listed in Table 5, the crystallite dimensions (L_c and L_a) of the carbon fibers increase in the order of C-MP-CFs < C/P-MP-CFs < P-MP-CFs. C-MP-CFs and P-MP-CFs show the highest mechanical properties and axial thermal conductivity, respectively, while C/P-MP-CFs possesses both high thermal conductivity and axial thermal conductivity. The properties and crystalline parameters of the carbon

fibers are in line with what could be expected from the XRD and Raman analyses of their precursor mesophase pitches, suggesting that the molecular structure and orientation of the mesophase pitches have significant influence on the mechanical properties and, particularly, the thermal conductivity of carbon fibers. The excellent mechanical properties of C-MP-CFs seem to result from the smaller oxygen uptake by their pre-oxidized fibers and a fine-grain strengthening effect [40]. On the other hand, the high axial thermal conductivity of P-MP-CFs was attributed to their large micro-texture size and that of their precursor [10,41]. Thus, the performance of carbon fiber can be considered to affected by both the chemical structure of its precursor and its crystallite dimensions. To sum up, the co-carbonization process makes that C/P-MP has the rigid aromatic mesogenic units and moderate short aliphatic chains molecular structure. The molecular structure control and the improvement of microcrystalline orientation of C/P-MP promote the prepared C/P-MP-CFs with both good mechanical properties and ultrahigh thermal conductivity to compare with those of the K13D2U commercial carbon fiber.

Table 5 Properties and crystal lattice parameters of the carbon fibers.

Sample	Properties					Crystal parameters		
	Elongation /%	TS /GPa	TM / GPa	ρ /$\mu\Omega\cdot$m	TC^n/ W/(m·K)	d_{002} /nm	L_a /nm	L_c /nm
C-MP -CFs	0.62	3.86	620	2.00	635	0.3375	44.30	25.96
C/P-MP-CFs	0.49	3.65	773	1.39	912	0.3370	56.12	29.84
P-MP-CFs	0.41	2.89	725	1.31	962	0.3369	63.65	39.96
K13D2U*	0.50	3.56	692	1.59	806	0.3371	54.90	27.02

[n] Thermal conductivity, calculated by the formula reported by Zhang [42].

*Commercial mesophase pitch-based carbon fiber manufactured by Mitsubishi Gas Chemical Co [43].

4. Conclusions

The structure and nature of raw materials have significant influence on the molecular structure of prepared mesophase pitches, and thus on the crystallite dimensions and performance of carbon fibers derived from the mesophase pitches. C-MP possessing the highest aromaticity, a rigid molecular structure and a very small amount of methyl groups makes C-MP-CFs with smaller crystal size and lower decomposition during the preparation process, thus results in best mechanical properties of their carbon fibers, consequently. P-MP's semi-rigid molecular structure and abundant methyl groups result in a certain degree of molecular plane distortion and good molecular mobility, respectively, which result in a mesophase pitch with the highest interlayer spacings and the largest crystallite dimensions. The largest crystallite dimension of P-MP combined with its higher molecular orientation makes P-MP-CFs possessing the highest crystal size and axial thermal conductivity. The C/P-MP-CFs, with both good mechanical properties and ultrahigh thermal conductivity have been prepared by co-carbonization of the coal tar and petroleum pitch raw material precursors. Their superior combination properties are attributed to C/P-MP's molecular structure which offers the advantages of both rigid aromatic mesogenic units and moderate short aliphatic chains inherited from the CP and PP, respectively.

References

21

[1] Matsumoto, T. *Pure Appl. Chem.* **1985,** 57 (11), 1553-62.

[2] Yue, Z.; Liu, C.; Vakili，A. *J. Mater. Sci* **2017**, 52 (13), 8176-8187.

[3] Barnes, A. B.; Dauché, F. M.; Gallego, N. C.; Fain, C. C.; Thies, M. C. *Carbon* **1998**, 36 (7-8), 855-860.

[4] Cheng, X. L.; Zha, Q. F.; Li, X. J.; Yang, X. J. *Fuel Process. Technol.* **2008**, 89 (12), 1436–1441.

[5] Mochida, I.; Korai, Y.; Oyama, T.; Nesumi. Y.; Todo, Y. *Carbon* **1989**, 27 (3), 359-365.

[6] Lou, B.; Liu, D.; Li, M.; Hou, X. L.; Ma, W. Q.; Lv, R. Q. *Energy Fuels* **2016**, 30 (2), 796-804.

[7] Greinke, R. A. *Carbon* **1990**, 28 (5), 701-706.

[8] Zhang, X. W.; Meng, Y. C.; Fan, B. L.; Ma, Z. K.; Song, H. H. *Fuel* **2019**, 243, 390-397.

[9] Mochida, I.; Shimizu, K.; Korai, Y.; Sakai, Y.; Fujiyama, S. *Bull. Chem. Soci. Japan* **1990**, 63 (10), 2945-2950.

[10] Mochida, I.; Shimizu, K.; Korai, Y.; Sakai, Y.; Fujiyama, S.; Toshima, H. *Carbon* **1992,** 30 (1), 55-61.

[11] Korai, Y.; Nakamura, M.; Mochida, I.; Sakai, Y.; Fujiyama, S. *Carbon* **1991**, 29 (4-5), 561-567.

[12] Yoon, S. H.; Korai, Y.; Mochida, I. *Carbon* **1993**, 31 (6), 849-856.

[13] Mochida, I.; Shimizu, K.; Korai, Y.; Otsuka, H.; Sakai, Y.; Fujiyama, S. *Carbon* **1990**, 28 (2-3), 311-319.

[14] Lee, S.; Eom, Y.; Kim, B. J.; Mochida, I.; Yoon, S. H.; Kim, B. C. *Carbon* **2015**, 81 (1), 694-701.

[15] Fan, X. H.; Fei, Y. Q.; Chen, L.; Li, W. *Energy Fuels* **2017**, 31 (5), 4694-4704.

[16] Kim, J. G.; Ji, H. K.; Song, B. J.; Jeon, Y. P.; Lee, C. W. Im, J. S. *Fuel* **2016**, 167, 25-30.

[17] Qian, S. A.; Zhang, P. Z.; Li, B. L. *Fuel* **1985**, 64 (8), 1085-1091.

[18] Guo, J. G.; Zhu, H.; Xu, H. T.; Aidan, W.; Li, X. K. *Energy Fuels* **2019**, 34(2): 2566-2573.

[19] Mora, E.; Santamarı́a, R.; Blanco, C.; Granda, M.; Mene´ndez, R. *J. Anal. Appl. Pyrol.* **2003**, 68-69 (03), 409-424.

[20] Mora, E.; Blanco, C.; Santamarı́a, R.; Granda, M.; Mene´ndez, R. *Carbon* **2003**, 41 (3), 445-452.

[21] Korai, Y.; Mochida, I. *Carbon* **1985**, 23 (1), 97-103.

[22] Park, Y. D.; Mochida, I. *Carbon* **1989**, 27 (6), 925−929.

[23] Díaz, C.; Blanco, C. G. *Energy Fuels* **2003**, 17 (4), 907-913.

[24] Liu, J. C.; Shimanoe, H.; Nakabayashi, K.; Miyawaki, J.; Ko, S.; Jeon, Y. P.; Yoon, S. H. *J. Indust. Eng. Chem.* **2018,** 67, 276-283.

[25] Yang, H.; Yoon, S. H.; Korai, Y.; Mochida, I.; Katou, O. *Chem. Lett.* **2002**, 2002 (6), 574-574.

[26] Siddiqui, M. N.; Ali, M. F.; Shirokoff, J. *Fuel* **2002**, 81 (1), 51-58.

[27] Feret, F. R. *Analyst* **1998**, 123 (4), 595-600.

[28] Li, M.; Liu, D.; Du, H.; Li, Q. Y.; Hou, X. L.; Ye, J. S. *Applied Petrochemical Research* **2015,** 5 (4), 339-346.

[29] Yuan, G. M.; Li, X. K.; Xiong, X. Q.; Dong, Z. J.; Aidan, W.; Li, B. L.; Ye, C.; Ma, G. Z.; Cui, Z. W.; Cong, Y.; Zhang, J.; Li, Y. J. *Carbon* **2017**, 115, 59-76.

[30] Alfe, M.; Apicella, B.; Tregrossi, A.; Ciajolo, A. *Carbon* **2008**, 46 (15), 2059-2066.

[31] Russo, C.; Stanzione, F.; Tregrossi, A.; Ciajolo, A. *Carbon* **2014**, 74 (8), 127-138.

[32] Mochida, I.; Toshima, H.; Korai, Y.; Varga, T. *J. Mater. Sci* **1990**, 25 (8), 3484-3492.

[33] Li, M.; Liu, D.; Men, Z.; Lou, B.; Yu, S. T.; Ding, J. W.; Cui, W. L. *Fuel* **2018,** 222, 617-626.

[34] Li, M.; Liu, D.; Lou, B.; Zhang, Y. D.; Yu, S. T.; Ding, J. W. *Rsc Adv.* **2018,** 8 (7), 3750-3759.

[35] Dumont. M.; Chollon, G.; Dourges, M. A. Pailler, R.; Bourrat, X.; Naslain, R.; Bruneel, J. L.; Couzi, M. *Carbon* **2002**, 40 (9), 1475-1486.

[36] Knight, D. S.; White, W. B. *J. Mater. Research* **1989**, 4 (2), 385-393.

[37] Matsumoto, T.; Mochida, I. *Carbon* **1992**, 30 (7), 1041-1046.

[38] Yanagida, K.; Sasaki, T.; Tate, K.; Saknish, A.; Korai, Y.; Mochida, I. *Carbon* **1993**, 31 (4), 577-582.

[39] Kim, B.; Kotegawa, T.; Eom, Y.; An, J.; Hong, I.; Kato, O.; Nakabayshi, K.; Miyawaki, J.; Kim, B.; Mochida, I.; Yoon, S. H. *Carbon* **2016,** 99, 649-657.

[40] Matsumoto, M.; Iwashita, T.; Arai, Y.; Tomioka, T. *Carbon* **1993**, 31 (5),715-720.

[41] Yoon, S. H.; Korai, Y.; Mochida, I.; Kato, I. *Carbon* **1994**, 32 (2), 273-280.

[42] Zhang, X.; Fujiwara, S.; Fujii, M. *Int. J. Thermo-physics* **2000**, 21 (4), 965-980.

[43] Emmerich, F. G. *Carbon* **2014**, 79 (1); 274-293.